13. Flemings, M. C. *Solidification Processing* (McGraw Hill, New York, 1974).
14. Swei, G. S., Lando, J. B., Reichert, S. E. & Mauritz, K. A. *Encyclopedia of Polymer Science and Engineering* Vol. 6, p. 209 (Wiley, New York, 1986).
15. Wittmann, J. C. & Lotz, B. Epitaxial crystallization of polymers on organic and polymeric substrates. *Prog. Polym. Sci.* **15,** 909–948 (1990).
16. Reiter, G. *et al.* Nanometer scale surface patterns with long range order created by crystallization of diblock copolymers. *Phys. Rev. Lett.* **83,** 3844–3847 (1999).
17. Smith, P. & Pennings, A. J. Eutectic crystallization of pseudo binary systems of polyethylene and high melting diluents. *Polymer* **15,** 413–419 (1974).
18. Wittmann, J. C., Hodge, A. M. & Lotz, B. Epitaxial crystallization of polymers onto benzoic-acid-polyethylene and paraffins, aliphatic polyesters, and polyamides. *J. Polym. Sci. Polym. Phys. Edn* **21,** 2495–2509 (1983).
19. Dorset, D. L., Hanlon, J. & Karet, G. Epitaxy and structure of paraffin-diluent eutectics. *Macromolecules* **22,** 2169–2176 (1989)
20. Wu, S. *Polymer Interface and Adhesion* (Marcel Dekker, New York, 1982).
21. Thomas, E. L. & Ast, D. Image intensification and the electron microscopy of radiation sensitive polymers. *Polymer* **15,** 37–41 (1974).
22. Kim, G. & Libera, M. Kinetic constraints on the development of surface microstructures in SBS thin films. *Macromolecules* **31,** 2670–2672 (1998).

Acknowledgements

We thank J.C. Wittmann, Y. Cohen, C. Thompson, C. Carter and L. Fetters for conversations; L. Fetters also synthesized the copolymer. This work was supported by the NSF, ACS-PRF and US-France NSF-CNRS.

Correspondence and requests for materials should be addressed to E.L.T. (e-mail: elt@mit.edu).

Large-scale synthesis of a silicon photonic crystal with a complete three-dimensional bandgap near 1.5 micrometres

Alvaro Blanco*†‡, Emmanuel Chomski§, Serguei Grabtchak*, Marta Ibisate†‡, Sajeev John*, Stephen W. Leonard*, Cefe Lopez†‡, Francisco Meseguer†‡, Hernan Miguez†‡, Jessica P. Mondia*, Geoffrey A. Ozin§, Ovidiu Toader* & Henry M. van Driel*

* *Department of Physics, 60 Saint George Street, University of Toronto, Toronto, Ontario, Canada M5S 1A7*
† *Unidad Asociada (CSIC-UPV) Universidad Politécnica, 46022 Valencia, Spain*
‡ *Instituto de Ciencia de Materiales de Madrid (CSIC), Cantoblanco 28049, Madrid, Spain*
§ *Department of Chemistry, 80 Saint George Street, University of Toronto, Toronto, Ontario, Canada M5S 3H6*

Photonic technology, using light instead of electrons as the information carrier, is increasingly replacing electronics in communication and information management systems. Microscopic light manipulation, for this purpose, is achievable through photonic bandgap materials[1,2], a special class of photonic crystals in which three-dimensional, periodic dielectric constant variations controllably prohibit electromagnetic propagation throughout a specified frequency band. This can result in the localization of photons[3–6], thus providing a mechanism for controlling and inhibiting spontaneous light emission that can be exploited for photonic device fabrication. In fact, carefully engineered line defects could act as waveguides connecting photonic devices in all-optical microchips[7], and infiltration of the photonic material with suitable liquid crystals might produce photonic bandgap structures (and hence light-flow patterns) fully tunable by an externally applied voltage[8–10]. However, the realization of this technology requires a strategy for the efficient synthesis of high-quality, large-scale photonic crystals with photonic bandgaps at micrometre and sub-micrometre wavelengths, and with rationally designed line and point defects for optical circuitry. Here we describe single crystals of silicon inverse opal with a complete three-dimensional photonic bandgap centred on 1.46 μm, produced by growing silicon inside the voids of an opal template of close-packed silica spheres that are connected by small 'necks' formed during sintering, followed by removal of the silica template. The synthesis method is simple and inexpensive, yielding photonic crystals of pure silicon that are easily integrated with existing silicon-based microelectronics.

Previously, three-dimensional photonic crystals have been fabricated in silicon by complex lithographic procedures which resulted in a thickness of only two unit cells in the growth direction[11,12]. Our materials synthesis, in contrast, begins with the highly controlled formation of a weakly sintered f.c.c. lattice of mono-disperse silica spheres whose diameter can be chosen between 600 and 1,000 nm. The silica opal structure is then used as a template for silicon infiltration. The large silica sphere size ensures that the final structure will have a complete photonic bandgap (PBG) in a wavelength range above the optical absorption edge (~1.1 μm) of bulk silicon. The synthesis of smaller (0.2–0.6 μm) sphere opals has been described previously[13]. The fabrication of periodically ordered opals with the larger unit cells involves the synthesis of mono-disperse (< 5% diameter variation) large spheres by a modified Stöber method[14]. The synthesis is performed in a suspension of smaller (500 nm diameter), mono-disperse silica particles that act as seeds for further growth; this leads to a homogeneous increase of the sphere size. Once the large spheres are made, they are settled in an aqueous solution of ethylene glycol (typically 50% concentration). The resulting opal is a close-packed f.c.c. lattice of silica spheres with a typical single domain size of 100 μm. A further sintering process leads to the formation of small necks between the silica spheres and

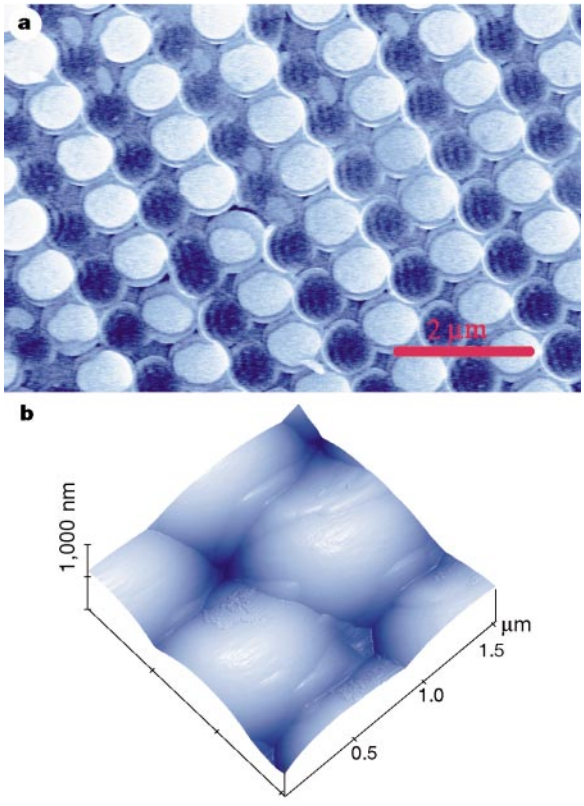

Figure 1 Silicon-infiltrated opal. **a**, SEM image of an internal [113] face of the silicon-infiltrated opal. The silica is indicated by light blue. **b**, AFM image of a 1.5 μm by 1.5 μm area of the infiltrated opal surface, highlighting the smoothness of the silicon coating.

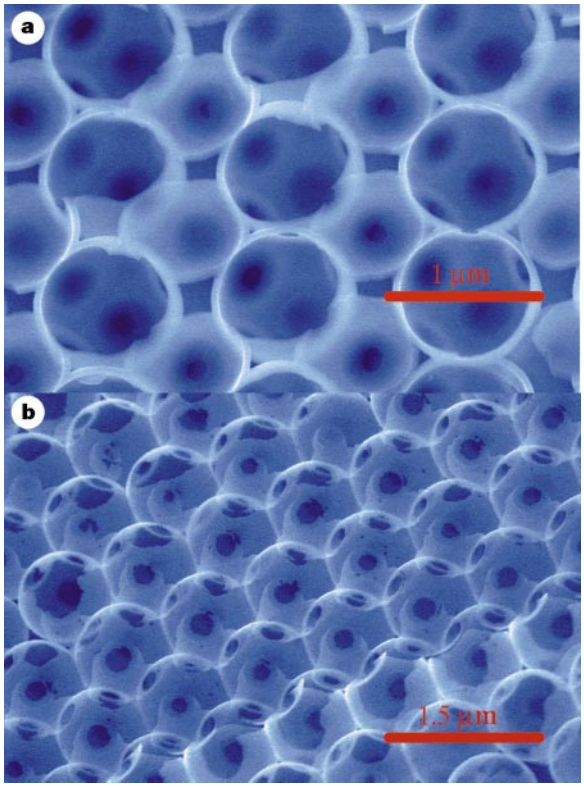

Figure 2 SEM images of internal facets of silicon inverse opal: **a**, [110] facet. **b**, [111] facet.

provides the template with mechanical stability. The necks also help to control the opal void volume for subsequent synthesis[15], and induce a connected network topology, allowing for removal of the template by an acid etching. This network topology also enhances optical scattering effects that are important for PBG formation[16].

Silicon is grown inside the voids of the opal template by means of chemical vapour deposition (CVD) using disilane (Si_2H_6) gas as a precursor[17,18]. Silane and disilane gas have both been used to grow silicon nanoclusters in periodic micro- and mesoporous silicas[7–19]. In our experiment, the deposition temperature is varied from 250 °C for low filling fractions to 350 °C for high ones. Our band structure calculations predict that the maximum PBG width is obtained with a 90–97% filling of the opal voids in the form of a uniformly thick wetting layer on the silica surfaces[16]. Samples with degrees of infiltration ranging up to 100% were synthesized. The reaction time was typically 24 hours and the disilane pressure was about 200 torr. After silicon growth, the samples are heated to 600 °C in order to improve the semiconductor crystallization and to allow diffusion of silicon inside the void structure. The silica template is subsequently removed using a fluoride-based etching procedure designed to minimize the dissolution of the macroporous silicon backbone.

Microscope Raman spectroscopy was used to ascertain the sample quality. A single phonon peak was observed in our samples centred at 519 cm^{-1} with a width less than 8 cm^{-1} consistent with the presence of crystalline silicon. Typical scanning electron microscopy (SEM) and atomic force microscopy (AFM) images of the infiltrated silica opal are shown in Fig. 1. The SEM image indicates a thick, uniform layer of silicon surrounding the well-ordered silica spheres (shown in light blue), indicating a high degree of infiltration. From the AFM image the silicon surface roughness is estimated to be less than 2 nm. The growth of the silicon-wetting layer is quite homogeneous and is independent of the local characteristics of the opal template. A SEM image of a typical inverse silicon opal taken after etching the infiltrated structure is shown in Fig. 2. The images reveal an interconnected network of air spheres surrounded by silicon shells, inheriting the f.c.c. order of the opal template. Adjacent air spheres are connected by windows, which result from the sintering process.

Unlike earlier inverse opal structures made of TiO_2 (refs 20, 21), graphitic carbon[22], CdSe and CdS (refs 23, 24), our silicon inverse opal structure simultaneously satisfies the two essential criteria for complete PBG formation. First, the refractive index of silicon (3.45 at 1.5 μm) is well above the theoretically determined[16] threshold (2.8) for a PBG in a f.c.c. lattice of air spheres. Second, the optical absorption edge of the silicon backbone occurs at a wavelength well below the PBG, thereby allowing coherent localization of light within the material with minimal absorptive losses. Such localization is an essential feature for PBG device applications; as light is caged within the dielectric microstructure, it cannot scatter into unwanted modes of free propagation and is forced to flow along engineered defect channels between devices integrated into an optical microchip.

The theoretically predicted photonic band structure of a silicon inverse opal, with 88% infiltration of silicon into the available volume of the opal template voids, is shown in Fig. 3. The calculations were performed using the plane-wave expansion method with a basis of 2662 plane waves[25]. As the infiltration level is numerically increased from 88% to 100%, the centre of the complete PBG moves from 1.46 to 1.55 μm, spanning the wavelength range of choice for fibre optic telecommunications.

The reflection and transmission spectra of a silicon inverse opal were measured using a Bomem Fourier transform infrared spectrometer. A microscope attached to the spectrometer was used to illuminate a single crystal domain with a high surface quality. Unpolarized light passed through the microscope produced a spot size ~40 μm in diameter with the incident light cone spanning 15°–35° from normal incidence. The resulting normalized reflection and transmission spectra are shown in Fig. 4. The reflection spectrum exhibits a broad peak with a centre wavelength of 2.5 μm with three

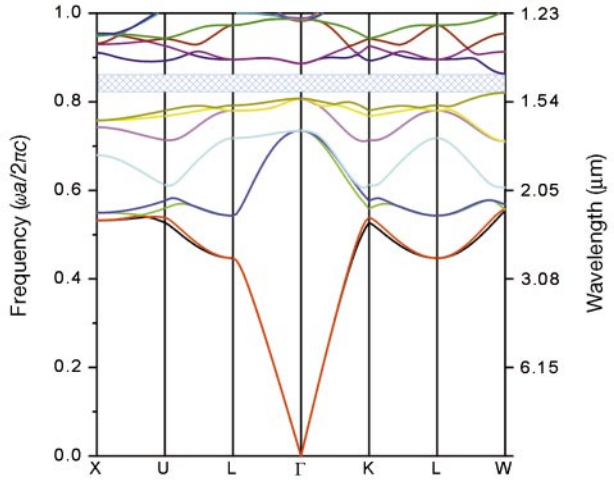

Figure 3 Band structure of silicon inverse opal with an 88% infiltration of Si into the available opal template voids. The complete photonic bandgap is shown by the crosshatched region, with a gap to mid-gap ratio of 5.1%.

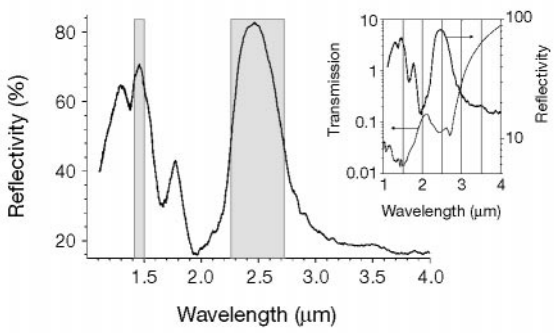

Figure 4 Reflection spectrum from the inverse silicon opal. Shaded regions at 2.5 μm and 1.5 μm show the calculated positions of the first stop band and the complete photonic bandgap, respectively. Inset, the transmission spectrum of the same sample on a logarithmic scale. The narrow transmission minimum at 2.7 μm is due to water absorption.

additional peaks between 1.2 and 1.8 μm. The reflectivity peak amplitude exceeds 80% and 70% at 2.5 μm and 1.46 μm, respectively, indicating good crystal quality. The sample transmission spectrum, indicated in the inset, has been corrected for diffuse scattering[26]. We note a strong correlation between the key spectral features of the transmission and reflectance data, that is, the maxima in the reflectance spectrum correspond to the minima in the transmission spectrum.

To compare the optical measurements to band structure calculations we first determined the lattice constant. This is preserved after infiltration and inversion, and was determined from reflectivity measurements of the bare opal at normal incidence. By comparing the spectral position of the first stop band edges (associated with the pseudogap at the L point of the first Brillouin zone[27]) to those predicted by band structure calculations (using a silica refractive index of 1.45), we obtained a (cubic) lattice constant of 1.23 μm.

The degree of infiltration was obtained by varying its value in the band structure calculation to obtain agreement with the centre wavelength of the first stop band, measured to be 2.5 μm. The silicon shell topology of Fig. 2 was assumed. One sees from Fig. 4 that the calculation gives the appropriate width for the stop band. Excellent agreement is also observed between the position of the peak in the reflectivity spectrum and the centre of the stop band at 1.46 μm, which is highly sensitive to the degree of infiltration. Calculations identify this band as the frequency interval associated with a complete bandgap. The good agreement between the measured spectra and the calculated band structure suggests the presence of a complete PBG centred at 1.46 μm, with a gap to mid-gap ratio of 5.1%. More comprehensive measurements are needed to provide full experimental verification of the photonic bandgap.

The synthesis of a very-large-scale, silicon-based PBG material offers a number of imminent possibilities, involving further infiltration of this highly open structure with light-emitting molecules or atoms. The resulting luminescence and lasing characteristics of light emitting species near a three-dimensional photonic band edge are expected to be quite striking. Important low-threshold all-optical switching effects and an anomalous nonlinear optical response have been predicted[25]. In this regard, it is useful to explore self-assembly methods for creating diamond lattice templates from which a considerably larger PBG may be achieved[28]. It is also important to generalize the template-formation procedure in order to engineer wave-guide channels and specified point defects through which light can flow. Methods of soft lithography and micromoulding in capillaries[29] may soon prove effective in realizing such 'circuits of light'. □

Received 31 January; accepted 14 April 2000.

1. John, S. Strong localization of photons in certain disordered dielectric lattices. *Phys. Rev. Lett.* **58,** 2486–2489 (1987).
2. Yablonovitch, E. Inhibited spontaneous emission in solid-state physics and electronics. *Phys. Rev. Lett.* **58,** 2059–2062 (1987).
3. John, S. Electromagnetic absorption in a disordered medium near a photon mobility edge. *Phys. Rev. Lett.* **53,** 2169–2172 (1984).
4. Anderson, P. W. The question of classical localization: A theory of white paint? *Phil. Mag. B* **52,** 505–509 (1985).
5. John, S. Localization of light. *Phys. Today* **44,** 32–40 (1991).
6. Wiersma, D. S., Bartolini, P., Lagendijk, A. & Righini, R. Localization of light in a disordered medium. *Nature* **390,** 671–673 (1997).
7. Joannopoulos, J. D.,Villeneuve, P. R. & Fan, S. Photonic crystals: putting a new twist on light. *Nature* **386,** 143–149 (1997).
8. Busch, K. & John, S. Liquid-crystal photonic-band-gap materials: The tunable electromagnetic vacuum. *Phys. Rev. Lett.* **83,** 967–970 (1999).
9. Yablonovitch, E. Liquid versus photonic crystals. *Nature* **401,** 539–541 (1999).
10. Leonard, S. W. *et al.* Tunable two-dimensional photonic crystals using liquid crystal infiltration. *Phys. Rev. B* **61,** 2389–2392 (2000).
11. Lin, S. Y. & Fleming, J. G. A. Three-dimensional optical photonic crystal. *IEEE J. Lightwave Technol.* **17,** 1944–1947 (1999).
12. Noda, S., Yamamoto, N., Imada, M., Kobayashi, H. & Okano, M. A three-dimensional optical photonic crystal. *IEEE J. Lightwave Technol.* **17,** 1948–1955 (1999).
13. Míguez, H. *et al.* Photonic crystal properties of packed submicrometric SiO_2 spheres. *Appl. Phys. Lett.* **71,** 1148–1150 (1997).
14. Stöber, W., Fink, A. & Bohn, E. Controlled growth of monodisperse silica spheres in the micron size range *J. Colloid Interface Sci.* **26,** 62–69 (1968).
15. Míguez, H. *et al.* Control of the photonic crystal properties of fcc packed submicrometer SiO_2 spheres by sintering. *Adv. Mater.* **10,** 480–483 (1999).
16. Busch, K. & John, S. Photonic band gap formation in certain self-organizing systems. *Phys. Rev. E* **58,** 3896–3908 (1998).
17. Chomski, E., Dag, Ö., Kuperman, A. & Ozin, G. A. New forms of luminescent silicon: silicon-silica composite mesostructures. *Chem. Vap. Dep.* **2,** 8–13 (1996).
18. Dag, Ö., Ozin, G. A., Yang, H., Reber, C. & Bussière, G. Photoluminescent silicon clusters in oriented hexagonal mesoporous silica film. *Adv. Mater.* **11,** 474–480 (1999).
19. Bogomolov, N. N. *et al.* Fabrication of regular three-dimensional lattices of submicron silicon clusters in a SiO_2 matrix. *Pis'ma Zh. Tekh Fiz.* **24,** 90–95 (1998); also *Technol. Phys. Lett.* **24,** 326–327 (1998).
20. Holland, B. T., Blanford, C. F. & Stein, A. Synthesis of macroporous minerals with highly ordered three-dimensional arrays of spheroidal voids. *Science* **281,** 538–540 (1998).
21. Wijnhoven, J. E. G. J. & Vos, W. L. Preparation of photonic crystals made of air spheres in titania. *Science* **281,** 802–804 (1998).
22. Zakhidov, A. A. *et al.* Carbon structures with three-dimensional periodicity at optical wavelengths. *Science* **282,** 897–901 (1998).
23. Vlasov, Y. A., Yao, N. & Norris, D. J. Synthesis of photonic crystals for optical wavelengths from semiconductor quantum dots. *Adv. Mater.* **11,** 165–169 (1999).
24. Braun, P. V. & Wiltzius, P. Electrochemically grown photonic crystals. *Nature* **402,** 603–604 (1999).
25. John, S. & Busch, K. Photonic bandgap formation and tunability in certain self-organizing systems. *J. Lightwave Technol.* **17,** 1931–1943 (1999).
26. Vlasov, Yu. A., Astratov, V. N., Karimov, O. Z. & Kaplyanskii, A. A. Existence of a photonic pseudogap for visible light in synthetic opals. *Phys. Rev. B* **55,** R13357–R13360 (1997).
27. Ashcroft, N. & Mermin, D. *Solid State Physics* 161 (Holt, Rinehart & Winston, New York, 1976).
28. Ho, K. M., Chan, C. T. & Soukoulis, C. M. Existence of a photonic gap in periodic dielectric structures. *Phys. Rev. Lett.* **65,** 3152–3155 (1990).
29. Xia, Y. & Whitesides, G. M. Soft lithography. *Angew. Chem. Int. Edn Engl.* **37,** 550–575 (1998).

Acknowledgements

This work was supported in part by the Natural Sciences and Engineering Research Council of Canada, Photonics Research Ontario, the Fundacion Ramon Areces, the Spanish CICyT project and the European Community Project. We are grateful to I. Sokolov and N. Coombs for their technical assistance with the AFM and SEM images (Figs 1 and 2).

Correspondence and requests for materials should be addressed to S. J. (e-mail: john@physics.utoronto.ca).

Deep convective clouds with sustained supercooled liquid water down to −37.5 °C

Daniel Rosenfeld* & William L. Woodley†

* *Institute of Earth Sciences, the Hebrew University of Jerusalem, Jerusalem 91904, Israel*

† *Woodley Weather Consultants, 11 White Fir Court, Littleton, Colorado 80127, USA*

In cirrus[1] and orographic wave clouds[2], highly supercooled water has been observed in small quantities (less than 0.15 g m^{-3}). This high degree of supercooling was attributed to the small droplet size and the lack of ice nuclei at the heights of these clouds[1,2]. For deep convective clouds, which have much larger droplets near their tops and which take in aerosols from near the ground, no such measurements have hitherto been reported. However, satellite data suggest that highly supercooled water (down to −38 °C) frequently occurs in vigorous continental convective storms[3]. Here we report *in situ* measurements in deep convective clouds from an aircraft, showing that most of the condensed water remains liquid down to −37.5 °C. The droplets reach a median volume diameter of 17 μm and amount to 1.8 g m^{-3}, one order of magnitude more than previously reported[2]. At slightly colder temperatures only ice was found, suggesting homogeneous freezing. Because of the poor knowledge of mixed-phase cloud processes[4], the simulation of clouds using numerical models is difficult at present. Our observations will help to understand these cloud processes, such as rainfall, hail, and cloud electrification, together with their implications for the climate system.

Cloud droplets do not readily freeze at 0 °C, but often remain liquid at colder temperatures in a "supercooled" state. Freezing of the cloud droplets can then be triggered by ice nuclei, or the droplets can freeze in an homogeneous fashion. The lowest temperatures at which pure water droplets can exist in a supercooled state for times longer than a fraction of a second before homogeneously freezing depends on the drop size. According to both theory[5] and laboratory experiments[6], a 10-μm cloud droplet freezes homogeneously near −39 °C. The coldest previously reported *in situ* measurements of supercooled liquid water content (SLWC) at temperatures below −32 °C, in excess of the sensitivity of the measuring instruments (0.02 g m^{-3} for hot-wire probes[7]), was 0.14 g m^{-3} at −36 °C in orographic lenticular wave clouds[2]. An SLWC of 0.06 g m^{-3} at the base of cirrus clouds, between −35° and −36 °C, was reported by Sassen[1], who stated that "in comparison with earlier reported aircraft measurements, the detection of such highly supercooled water is unique".

Both reports[1,2] suggested that the dearth of ice nuclei derived from the Earth's surface in the upper troposphere prevented heterogeneous nucleation, allowing for the observed homogeneous nucleation at such cold temperatures in altocumulus and cirrus clouds[8]. No previous reports are available for observations of similar highly supercooled water and homogeneous freezing in convective clouds with roots near the surface. In view of the reported findings to the contrary here, we can only speculate about the reasons they have not been reported previously. Perhaps low priority was given to such measurements, because it was felt that clouds taking in air rich in ice nuclei from the boundary layer would glaciate long before reaching the point of homogeneous freezing[9]. Or perhaps such measurements were not made because of the safety problems involved in penetrating vigorous cumulonimbus towers at the −30 to −40 °C isotherm levels in storms that typically contain hail and frequent lightning.

The first indications available to us that highly supercooled water might exist in convective clouds were obtained by remote sensing from satellites over Thailand, using the technique reported in ref. 3. The inference of supercooled water at temperatures below −30 °C prompted us to fly with the Thai King Air cloud-physics aircraft to measure the cloud microstructure in Thailand clouds. Penetrating feeders of cumulonimbus clouds, an SLWC of 2.4 g m^{-3} was measured at the operational ceiling of the aircraft (9,300 m above sea level, a.s.l.) at a temperature of −31.6 °C (ref. 10). The cloud-base temperature was +13 °C at 2,800 m a.s.l., and the SLWC was measured by the King hot-wire instrument.

Analysis of the satellite data using the methodology of Rosenfeld and Lensky[3] suggested that supercooled water occasionally occurred at temperatures approaching −40 °C in cumulonimbus clouds over the western USA. An opportunity to validate these satellite inferences came when Weather Modification Inc. gave us access to its Lear jet cloud-physics aircraft in the period 9–14 August 1999 for measurements in Texas clouds. The aircraft cloud-physics instrumentation included the following: (1) a hot-wire cloud liquid water probe, model LWC-100 (Droplet Measurement Technologies). The measurement efficiency of the sensor depends on the drop sizes. For the observed distribution, it underestimated the SLWC by not more than 10%. (2) An air temperature probe, model 102AU1AP (Rosemount). (3) A forward scattering spectrometer probe (FSSP) for droplet sizes in the range 0.5–47 μm, model FSSP-100 (Particle Measuring Systems Inc). (4) An optical array particle imaging probe, for the range 25—800 μm, model OAP-2D2-C (Particle Measuring Systems, Inc.).

High-altitude measurements in the tops of vigorous growing convective elements of cumulonimbus clouds were done with the Lear jet on 11 and 13 August 1999. The visibly most-vigorous new convective elements were measured as they grew through the measurement flight level. In addition, extensive measurements were made at all levels down to the cloud base, in order to document the vertical microphysical evolution of the cloud. Cloud base on both days was near 3,500 m a.s.l. at a temperature of 10 °C.

On the flight of 11 August (20:28–23:42 GMT) just to the west of Lubbock, Texas (34° N, 102° W), an SLWC of 0.6 g m^{-3} was observed at −35.9 °C, 0.9 g m^{-3} at −35.6 °C, and 1.5 g m^{-3} at −34.4 °C. Larger values of SLWC, up to 2.4 g m^{-3}, were recorded at warmer cloud temperatures. Direct measurements of the updraught velocity were not available. However, a rate of climb of 6 m s^{-1} was sufficient to keep up with the rate of growth of the tops of some of the clouds containing highly supercooled water. The residence time of the water was measured by repeated penetrations in the same cloud, which was narrow and clearly isolated. In three passes spaced at 3.5-min intervals, the temperatures and maximum cloud water contents were 1.2 g m^{-3} at −32.9 °C, 1.5 g m^{-3} at −32.7 °C, and 0.4 g m^{-3} at −35.2 °C. This means that the large amounts of highly supercooled cloud water were not a transient feature, but rather were long lasting, with freezing time of about 7 min.

On the flight of 13 August (20:26–23:09 GMT), to the north of Midland, Texas (33°N 102°W), effort was focused on documentation of the transition from water clouds to ice clouds in vigorous convective elements. Extensive documentation of the clouds from